nature nanotechnology

SUPPLEMENTARY INFORMATION

https://doi.org/10.1038/s41565-020-0715-4

In the format provided by the authors and unedited.

Quantum Hall effect of Weyl fermions in n-type semiconducting tellurene

Gang Qiu[1,2], Chang Niu[1,2], Yixiu Wang[3], Mengwei Si[1,2], Zhuocheng Zhang[1,2], Wenzhuo Wu[3] and Peide D. Ye[1,2]✉

[1]School of Electrical and Computer Engineering, Purdue University, West Lafayette, IN, USA. [2]Birck Nanotechnology Centre, Purdue University, West Lafayette, IN, USA. [3]School of Industrial Engineering, Purdue University, West Lafayette, IN, USA. ✉e-mail: yep@purdue.edu

Supplementary Information for:

Quantum Hall Effect of Weyl Fermions in Semiconducting *n*-type Tellurene

Gang Qiu[1,2], Chang Niu[1,2], Yixiu Wang[3], Mengwei Si[1,2], Zhuocheng Zhang[1,2], Wenzhuo Wu[3] and Peide D. Ye[1,2]

List of contents

Supplementary Fig. 4: ρ_{xx} and $\Delta\sigma_{xx}$ comparison at various carrier density.

Supplementary Fig. 5: Oscillation phase factor extracted from $\Delta\sigma_{xx}$ and ρ_{xx}.

Supplementary Fig. 6: SdH oscillations in a tilted magnetic field.

Supplementary Fig. 7: Extracting Berry phase using SdH oscillation phase offset from 8 more devices.

Supplementary Fig. 8: Weak anti-localization effect in n-type Te films.

<u>Supplementary Note 1</u>: Additional data from other devices on quantum Hall effects and Shubnikov-de Haas oscillations

To demonstrate the reproducibility of our experimental results, here we present the complete set of data from another high-mobility device. Supplementary Fig. 1 shows the longitudinal (R_{xx}) and Hall (R_{xy}) resistance measured at 1.7 K up to 31 Tesla. This device also reaches the quantum Hall states at filling factor υ=4. The SdH oscillation pattern mapping in Supplementary Fig. 2 shows similarity to the device presented in our main manuscript. Temperature-dependent SdH amplitudes were measured to extract the cyclotron mass (see Supplementary Fig. 3) which is in accordance with our previous results. Additionally, extraction of the oscillation phase offset from 8 more devices is presented in Supplementary Note 4.

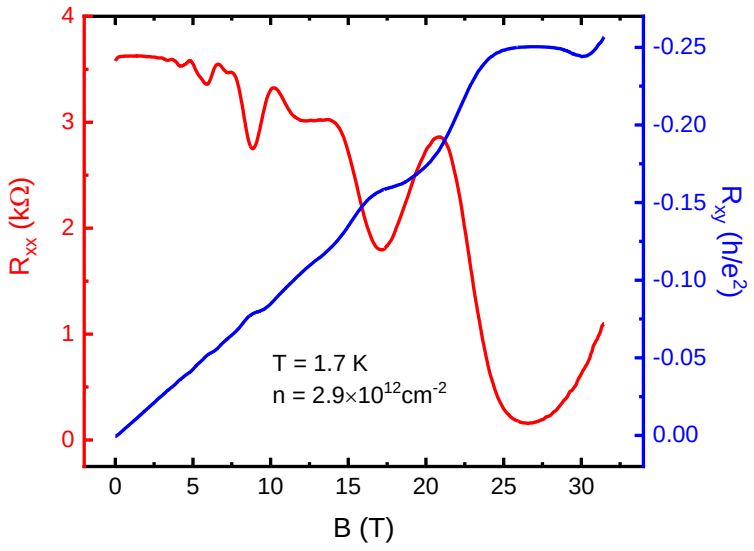

Supplementary Fig. 1| Quantum Hall effect of another high mobility sample. Longitudinal (R_{xx}, red) and transverse (R_{xy}, blue) resistance measured under magnetic field up to 31.4 T at 1.7 K.

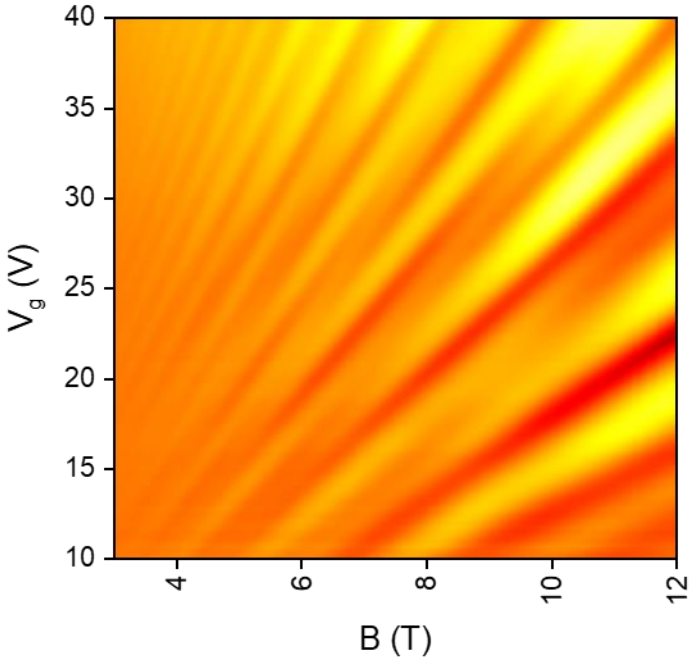

Supplementary Fig. 2| R_{xx} mapping of another high mobility sample in Vg-B parameter space.

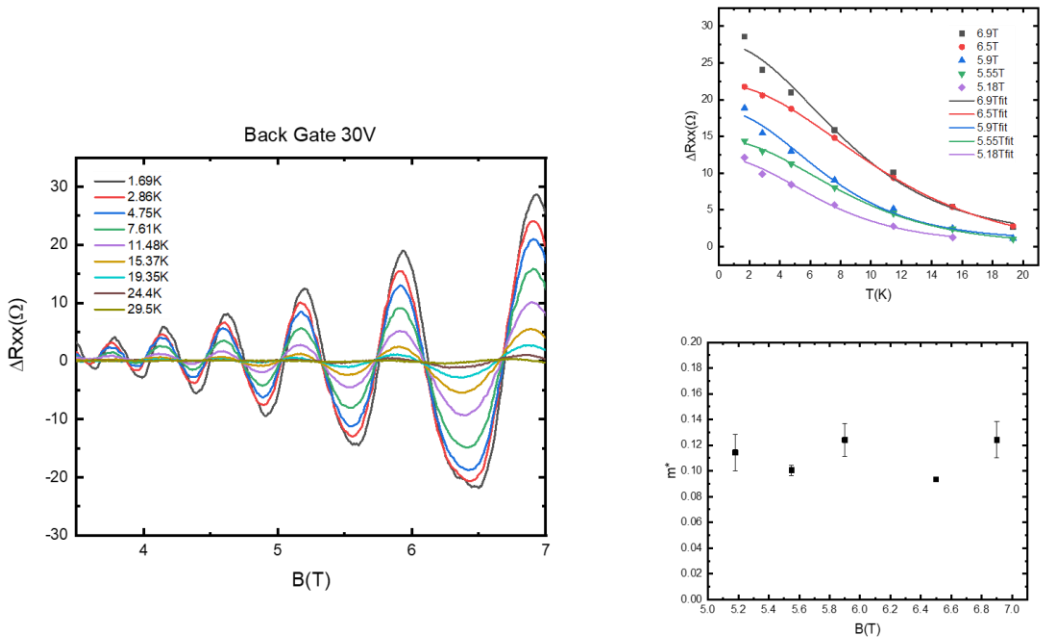

Supplementary Fig. 3| Temperature-dependent SdH oscillations and extraction of cyclotron mass of another high mobility sample.

Supplementary Note 2: Converting Hall resistivity to Hall conductivity with anisotropic Hall tensor

Although historically it is a common practice to extract the oscillation phase offset from the longitudinal resistivity (ρ_{xx})[1,2], it is argued that the fundamental quantization occurs in the conductivity instead of resistivity[3,4]. Hence using ρ_{xx} instead of σ_{xx} can be risky and will sometimes lead to a phase shift[5]. Here we first convert the Hall resistivity into conductivity using the anisotropic Hall tensor and then evaluate the phase offsets extracted using both methods.

Due to its unique atomic structure, the conductivity of Te is highly anisotropic. Extra caution needs to be taken when we apply the Hall tensor to convert from the resistivity matrix to the conductivity matrix. The resistivity ratio $\eta = \rho_{xx}/\rho_{yy} = 1.4$ was previously determined through transport measurements[6,7]. The inverse of the resistivity matrix gives $\begin{pmatrix} \sigma_{xx} & \sigma_{xy} \\ \sigma_{yx} & \sigma_{yy} \end{pmatrix} = \begin{pmatrix} \rho_{xx} & \rho_{xy} \\ \rho_{yx} & \frac{1}{\eta}\rho_{xx} \end{pmatrix}^{-1}$, and subsequently we have $\sigma_{xx} = \frac{\eta\rho_{xx}}{{\rho_{xx}}^2+\eta{\rho_{xy}}^2}, \sigma_{xy} = \frac{\rho_{xy}}{{\rho_{xx}}^2+\eta{\rho_{xy}}^2}$.

Next, we shall evaluate whether using resistivity to construct the Landau fan diagram and extract phase offset is reliable in the case of Te. For some semimetals, because of their high carrier density, the extreme condition $\sigma_{xx} \gg \sigma_{xy}$ gives $\sigma_{xx} \propto \rho_{xx}^{-1}$, hence this will completely flip the phase. However, in our semiconductor system, this extreme condition does not hold. By plotting ρ_{xx} and $\Delta\sigma_{xx}$ (subtracting a smooth background) over a wide gate voltage range (Supplementary Fig. 4), we immediately notice that the minima in both curves coincide, suggesting that the phase shift using ρ_{xx} in this case is negligible and will not undermine our conclusion. As a matter of fact, we notice that using $\Delta\sigma_{xx}$ in the LL fan diagram gives us a slight edge in reliably extracting the phase factor (Supplementary Fig. 5). Hence in the main manuscript, the phase offset is extracted using σ_{xx} for correctness, and the rest of the phase offsets included in Supplementary Note 4 are extracted from ρ_{xx} for simplicity.

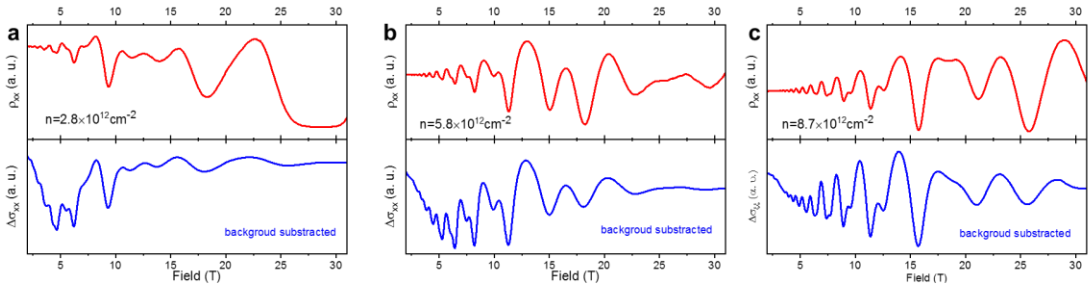

Supplementary Fig. 4| ρ_{xx} and $\Delta\sigma_{xx}$ comparison at various carrier density. ρ_{xx} and $\Delta\sigma_{xx}$ (subtracting a smooth background) at carrier density **(a)** 2.8×10^{12} cm^{-2}, **(b)** 5.8×10^{12} cm^{-2}, and **(c)** 8.7×10^{12} cm^{-2}. The minima in ρ_{xx} and $\Delta\sigma_{xx}$ coincide in all three situations.

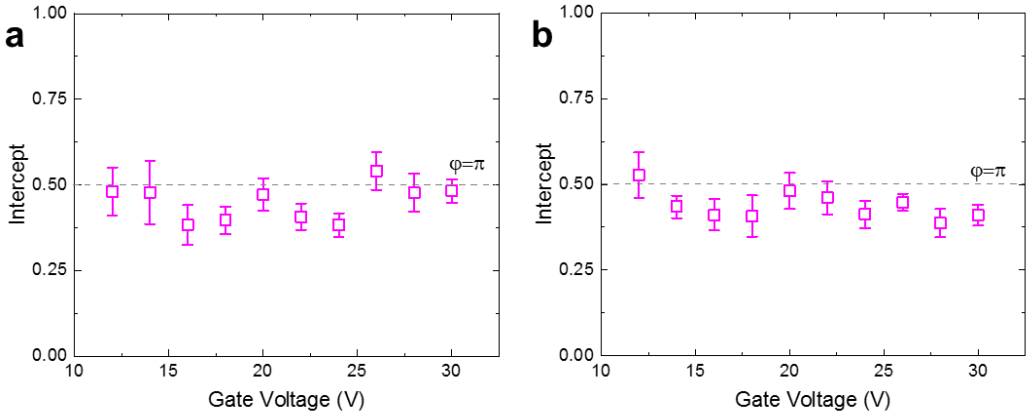

Supplementary Fig. 5| Oscillation phase factor extracted from (a) $\Delta\sigma_{xx}$ and (b) ρ_{xx}.

Supplementary Note 3: Shubnikov-de Haas oscillations in tilted magnetic field

To extract the effective g-factor, SdH oscillations are measured under tilted magnetic fields to disentangle the cyclotron energy $E_C = \frac{\hbar e B_\perp}{m^*}$ and the Zeeman energy $E_Z = g^*\mu_B B_{total}$. By rotating the sample to certain angles, one should expect to see the coincidence effect – the exchange of SdH maxima and minima under the condition $E_C = E_Z$. Here we measured

our sample in tilted magnetic field, however coincidence effect was not observed until 78.2º (see Fig. S6), from which we can estimate the upper bound of the effective g-factor to be 2.68. The real g* may be even smaller given the fact that no clear trace of developing coincidence effect is observed until such a high angle. This suggests that the Zeeman energy in Te is much smaller than the cyclotron energy, ruling out a possible source of phase shift seen in the case of WSe_2[8] or n-type black phosphorous[9].

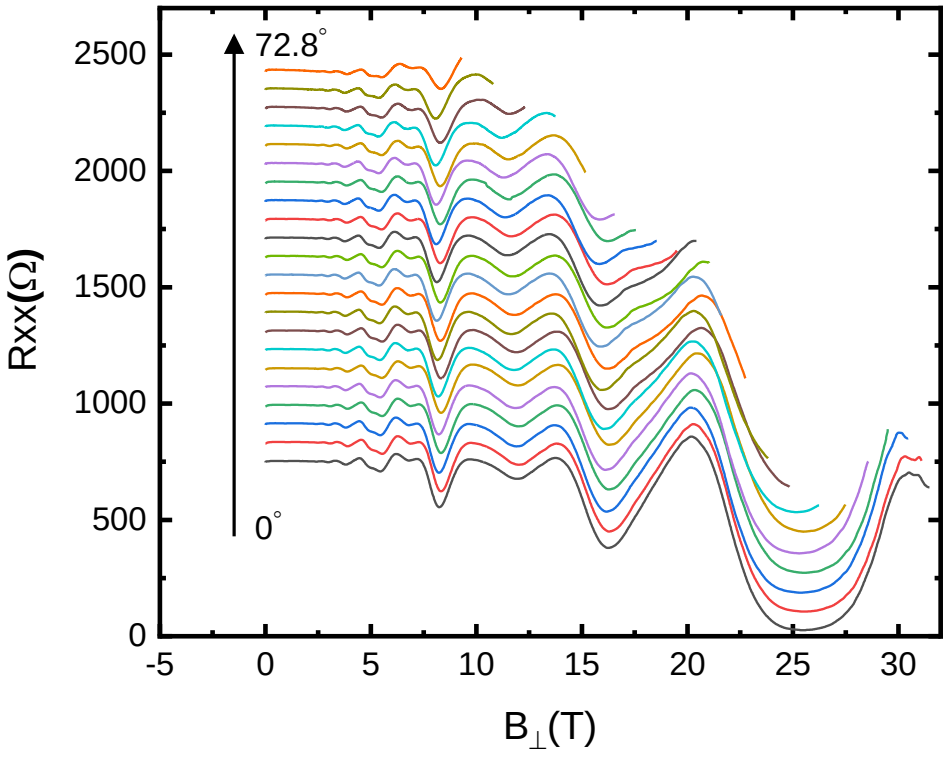

Supplementary Fig. 6| SdH oscillations in a tilted magnetic field. The curves are separated by 80 Ω offset for clarity. No evidence of coincidence effect is observed, suggesting a small effective g-factor.

<u>Supplementary Note 4</u>: More data on extracting Berry phase

The way we extract Berry phase relies on accurately reading R_{xx} minima at each filling factor. Here we only use the SdH oscillation periods where the degeneracy is not lifted, and all the minima are extracted from the predominant set of oscillations. However, even the splitting is not resolvable at low magnetic fields, and there is a chance that the energy splitting within the Landau levels can deviate R_{xx} minima and cause misinterpretations when extracting the Berry phase. To eliminate this uncertainty, we extracted Landau fan diagram intercepts for another 8 devices as shown in Fig. S7, and all of them unanimously show a π phase shift. This is solid proof that the phenomenon reported in the main paper is reproducible, and our method of extracting Berry phase is reliable.

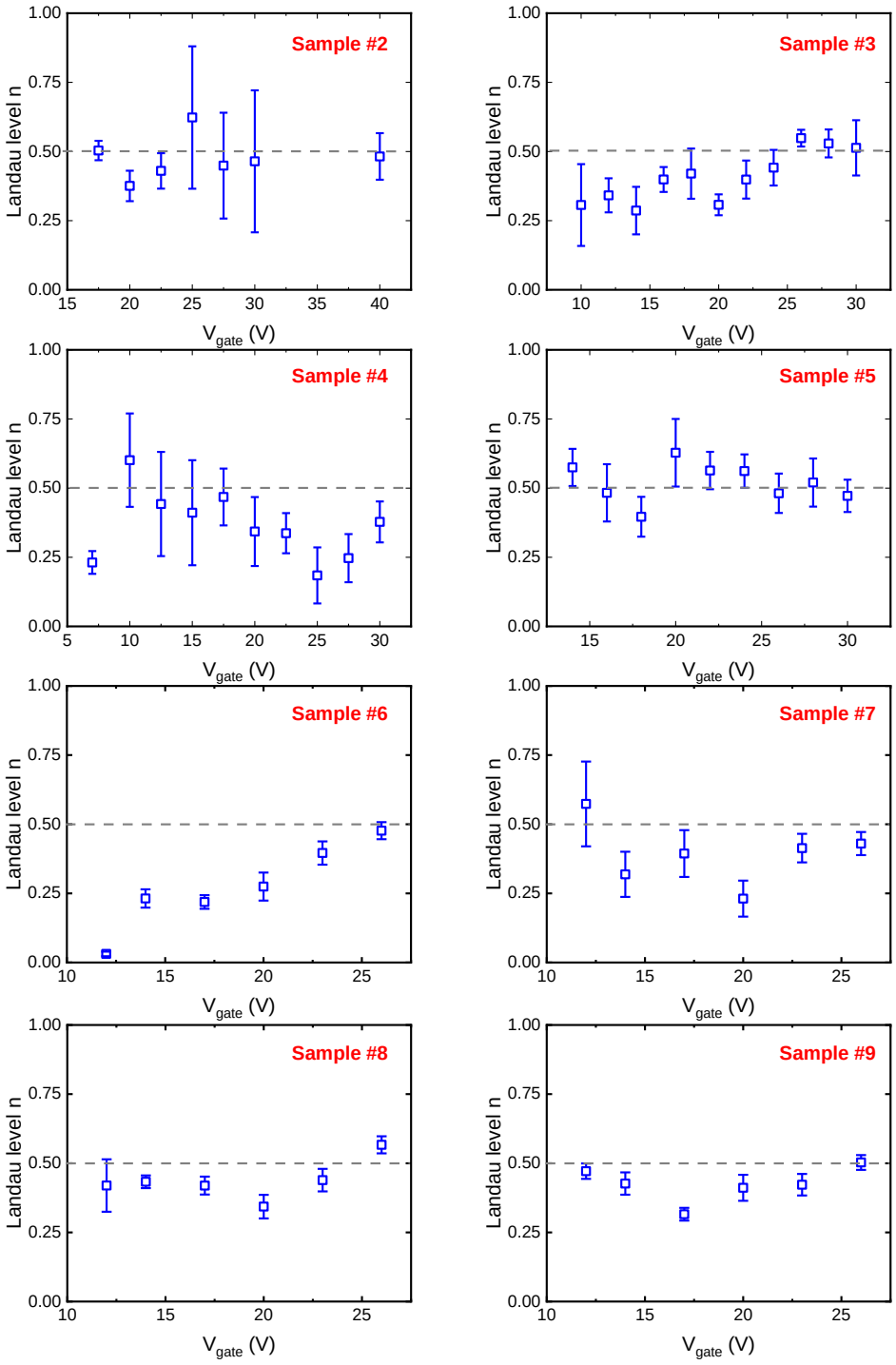

Supplementary Fig. 7| Extracting Berry phase using SdH oscillation phase offset from 8 more devices.

.

Supplementary Note 5: Weak anti-localization in n-type Te films

Weak anti-localization (WAL) is a phenomenon in the low B field regime that causes the resistance of a material to show a dip centered at zero. In normal materials there should be a peak in resistance at zero field, since the magnetic field destroys the localization effect and reduces the resistivity of the material, which is referred to as the weak localization effect. However, in systems with strong spin-orbit coupling, the trajectory of the electrons travelling around the disorder clockwise and counterclockwise will contribute a negative sign to the wavefunction and the constructive interference will reduce the resistivity. WAL in p-type Te films has been reported in previous work[10,11]. Here we show some preliminary WAL data in n-type Te films in Fig. S8 to verify strong SOC in the Te system. More comprehensive analysis of n-type Te WAL effects is beyond the scope of this work and will be reported independently[12].

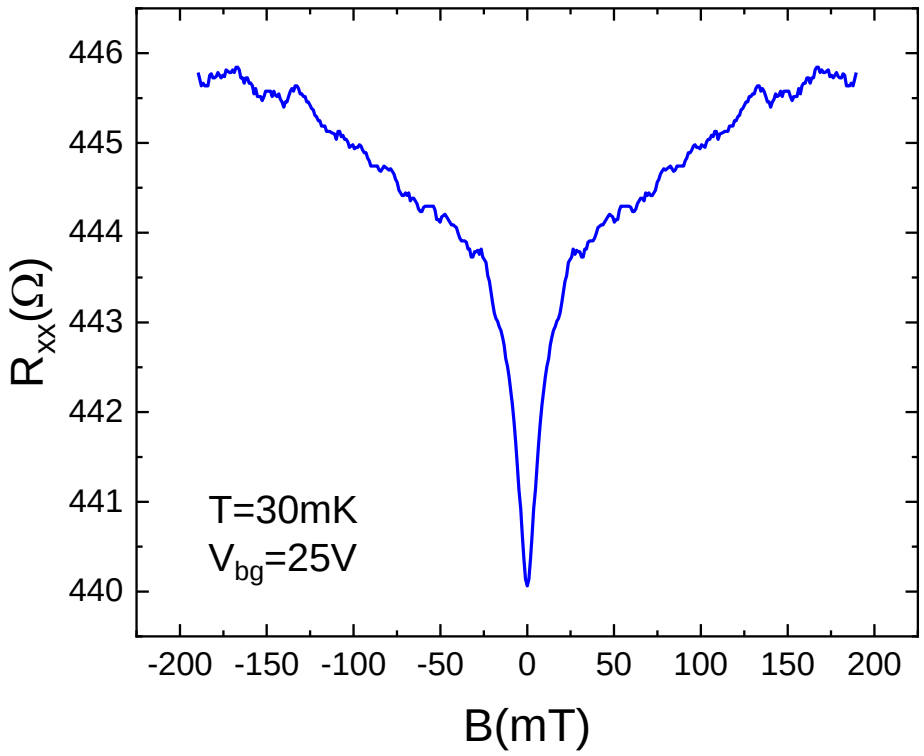

Supplementary Fig. 8| The weak anti-localization effect in n-type Te films.

1. Zhang, Y. B., Tan, Y. W., Stormer, H. L. & Kim, P. Experimental observation of the quantum Hall effect and Berry's phase in graphene. *Nature* **438**, 201–204 (2005).

2. Novoselov, K. S. *et al.* Two-dimensional gas of massless Dirac fermions in graphene. *Nature* **438**, 197–200 (2005).

3. Xiong, J. *et al.* Quantum oscillations in a topological insulator Bi_2Te_2Se with large bulk resistivity (6Ωcm). *Phys. E Low-dimensional Syst. Nanostructures* **44**, 917–920 (2012).

4. Ando, Y. Topological Insulator Materials. *J. Phys. Soc. Japan* **82**, 1–32 (2013).

5. Ren, Z., Taskin, A. A., Sasaki, S., Segawa, K. & Ando, Y. Large bulk resistivity

and surface quantum oscillations in the topological insulator Bi_2Te_2Se. *Phys. Rev. B* **82**, 241306 (2010).

6. Wang, Y. *et al.* Field-effect transistors made from solution-grown two-dimensional tellurene. *Nat. Electron.* **1**, 228–236 (2018).

7. Qiu, G. *et al.* Quantum transport and band structure evolution under high magnetic field in few-layer tellurene. *Nano Lett.* **18**, 5760–5767 (2018).

8. Xu, S. *et al.* Odd-Integer quantum Hall states and giant spin susceptibility in p - type few-layer WSe_2. *Phys. Rev. Lett.* **118**, 067702 (2017).

9. Li, L. *et al.* Quantum oscillations in a two-dimensional electron gas in black phosphorus thin films. *Nat. Nanotechnol.* **10**, 608–613 (2015).

10. Du, Y. *et al.* One-dimensional van der Waals material tellurium: Raman spectroscopy under strain and magneto-transport. *Nano Lett.* **17**, 3965−3973 (2017).

11. Ren, X. *et al.* Gate-tuned insulator-metal transition in electrolyte-gated transistors based on tellurene. *Nano Lett.* **19**, 4738–4744 (2019).

12. Niu, C. *et al.* Gate-tunable Strong Spin-orbit Interaction in Two-dimensional Tellurium Probed by Weak-antilocalization. *arXiv Prepr. arXiv1909.06659* (2019).